AGU PUBLICATIONS

JGR

Journal of Geophysical Research: Atmospheres

RESEARCH ARTICLE
10.1002/2017JD026548

Key Points:
- An experimental method enabled the isolation of black carbon from $PM_{2.5}$, and BC absorption enhancement was determined
- A climate model was configured with the observed absorption enhancement from coating effect
- BC radiative forcing doubled due to mixing with nonabsorbing aerosols, improvement in model, and AERONET observations of AAOD

Supporting Information:
- Supporting Information S1

Correspondence to:
B. Chen,
bingchen@sdu.edu.cn

Citation:
Chen, B., Z. Zhu, X. Wang, A. Andersson, J. Chen, Q. Zhang, and Ö. Gustafsson (2017), Reconciling modeling with observations of radiative absorption of black carbon aerosols, *J. Geophys. Res. Atmos.*, *122*, doi:10.1002/2017JD026548.

Received 24 JAN 2017
Accepted 5 MAY 2017
Accepted article online 11 MAY 2017

Reconciling modeling with observations of radiative absorption of black carbon aerosols

Bing Chen[1,2], Zhejing Zhu[1], Xinfeng Wang[1], August Andersson[3], Jianmin Chen[1], Qingzhu Zhang[1], and Örjan Gustafsson[3]

[1]Environmental Research Institute, Shandong University, Jinan, China, [2]Collaborative Innovation Center of Climate Change, Jiangsu, China, [3]Department of Environmental Science and Analytical Chemistry (ACES) and the Bolin Centre for Climate Research, Stockholm University, Stockholm, Sweden

Abstract The physical treatment of internal mixing and aging of black carbon (BC) aerosols that allow for enhanced solar absorption of the BC is an important parameterization in climate models. Many climate models predict a factor of 2–3 lower aerosol absorption optical depth (AAOD) than the atmospheric columnar absorption observed from ground-based networks such as AERONET, likely because these models do not parameterize properly the BC absorption enhancement (E_{MAC}). Models that are configured with an internal mixing have predicted large variations of E_{MAC}, which are poorly constrained from ambient measurements. We determined the BC E_{MAC} from aerosol coatings with a two-step solvent experiment to remove both organic and inorganic coatings in ambient fine particulate matter ($PM_{2.5}$). Observations in a rural North China site showed that the E_{MAC} varied from 1.4 to 3. The E_{MAC} increases simultaneously with SO_4^{2-}/EC ratios, suggesting the photochemical production of sulfate coatings enhanced BC absorption. A global climate model, parameterized to account for these observational constraints, verifies that sulfates are primary drivers of the BC absorption enhancement in severely polluted area in China. This magnification of the radiative forcing of coated BC is stronger by a factor of ~2 than predicted by the standard parameterization (external mixing) in the climate model and is in better agreement with AERONET observations of AAOD. This result would be useful for testing the representation of solar absorption by BC-containing particles in the newer generation of climate models.

Plain Language Summary Atmospheric black carbon (BC) or soot in fine particulate matter (PM2.5) is emitted from incomplete combustion of fossil fuel or biomass/biofuel. The BC is an important pollutant for both air quality and Earth's energy balance, and the BC radiative forcing maybe second only to that of CO_2. The photochemical production of nonabsorbing secondary aerosols may create a coating on BC and may thereby act as a lens which may enhance the light absorption. However, this absorption enhancement is poorly constrained by ambient measurements, and thus the estimates of BC climate forcing remain highly uncertain. To this end, an aerosol filter dissolution-filtration (AFD) with two-step solvent dissolution protocol was employed to remove both organic and inorganic coatings and then investigate their effects on BC light absorption. The observations and model simulation showed that the BC warming effect likely doubled due to lens effect from secondary aerosols.

1. Introduction

Atmospheric black carbon (BC) is the highly condensed residue of incomplete combustion of biomass/biofuel and fossil fuel. Uncertainties in the net radiative forcing due to the BC have been implicated in the current factor of 2–3 underprediction in aerosol absorption optical depth (AAOD) of many climate models compared to observations of atmospheric columnar absorption based on ground-based networks such as AERONET [*Andreae and Ramanathan*, 2013; *Cohen and Wang*, 2014; *Shindell et al*., 2013b]. The observation-model discrepancy is partly attributed to the physical treatment of internal mixing and aging of BC aerosol or optical focusing that allows enhanced absorption of the BC [*Jacobson*, 2000, 2001].

The model performance can be improved through refining BC emission inventory and observational constraints of BC absorption enhancement after mixing with non-BC aerosol components in the atmosphere [*Cohen and Prinn*, 2011; *Schulz et al*., 2006]. In Asia, emission inventories are recently improved by fine resolution, intensive investigation of energy consumption, and refining emission factors [*Cohen and Wang*, 2014;

Kurokawa et al., 2013; *Lu et al*., 2011; *Qin and Xie*, 2012], which in turn improves the simulation of atmospheric BC concentration [*Cohen*, 2014; *Koch et al*., 2009; *Zhang et al*., 2015].

The accurate configuration of BC absorption enhancement (E_{MAC}) due to aerosol mixing states (coating effect) may contribute to 3 times of sensitive ranges compared to BC mass uncertainties in East Asia [*Matsui*, 2016]. A model using internal mixing and enhanced absorption of BC shows no underestimation for the AERONET and OMI (Ozone Monitoring Instrument) AAOD [*Jacobson*, 2012]. Climate models vary widely in describing BC aerosols to be either externally or internally mixed [*Chung and Seinfeld*, 2005; *He et al*., 2014; *Schulz et al*., 2006], or using a more physically intuitive approach [*Cohen and Wang*, 2014; *Cohen et al*., 2011]. Laboratory experiments suggest that depending on shell thickness of coating matters, BC absorption can be enhanced by a factor of 1 to 4 (Table S1 in the supporting information). However, the laboratory experiments and model predictions have been poorly constrained [*Gustafsson and Ramanathan*, 2016], because the ambient measurements of E_{MAC} are challenging [*Cappa et al*., 2012; *Fierce et al*., 2016; *Peng et al*., 2016].

In this study, we employed an aerosol filter dissolution-filtration (AFD) method for experimentally removing the coating materials in ambient BC-containing aerosols. Samples of fine particulate matter ($PM_{2.5}$) in North China were treated by the AFD decoating method. Then, the mass absorption cross section (MAC) of BC was calculated for the filter-collected aerosols before and after the AFD decoating treatment. The ratio of MAC of ambient aerosol samples and their decoated BC isolates represents the absorption enhancement (E_{MAC}) of BC due to coatings in ambient aerosols. We then applied these E_{MAC} in a climate model simulation from the Coupled Model Intercomparison Project Phase 5 (CMIP5). The enhanced simulation was compared to the AERONET observations to test the AAOD prediction.

2. Determination of BC Absorption Enhancement in Ambient Aerosols

2.1. Field Campaign

Observational constraints of BC absorption enhancement from ambient aerosol coatings were performed at a regional rural site (36.83°N, 116.57°E) in the center of the North China Plain (NCP). The observation site was in small grassland patches surrounded by wheat farmland. Vegetation cover sheltered the site from surface soil dust emission. Local agriculture waste burning in the sampling area was not observed during the campaign. Several houses were located about 1 km away, and gas cooker might have a contribution for local emissions.

The monitors and sampling inlets were set at 1.5–3 m high above ground level with the support from a temporary field station (Figure S1). $PM_{2.5}$ samples were collected on precombusted quartz filters (90 mm in diameter, Pallflex, Tissuquartz 2500 QAT-UP) mounted on midvolume (100 L min^{-1}) atmospheric samplers (TH-150C-III, Wuhan Tianhong Instrument Co., Ltd, China). The samples were collected during daytime (9:00 A.M. to 17:00 P.M.) and night (17:30 P.M. to 8:30 A.M.) for each day in three weeks of June and July 2014; 21 daytime samples and 21 night samples were obtained. The concentrations of water-soluble inorganic ions (SO_4^{2-}, NO_3^-, and NH_4^+) in $PM_{2.5}$ were measured by a model ADI 2080 online analyzer for Monitoring for AeRosols and Gases (MARGA, Applikon Analytical B.V., the Netherlands) at 1 h time resolution [*Du et al*., 2011]. Meanwhile, the 1 h resolution concentrations of elemental carbon (EC) and organic carbon (OC) were measured by an online ECOC analyzer.

2.2. AFD Water and Organic Solvent Treatment

The aerosol filter filtration-dissolution (AFD) method removes non-BC substances from the sample filters by two stages of dissolution mediated by water and organic solvents. Water dissolves sulfate, nitrate, ammonium, and water-soluble organic carbon in filter aerosol samples. The remaining organic carbon (OC) on the filter is removed with dichloromethane (DCM) and acetone mixtures [*Rajput and Sarin*, 2014]. The two-stage solvent treatments dissolved all water-soluble salts and ~90% organic carbon in the aerosol samples. The AFD system thus enables the decoating of BC, with recovery of ~99% of EC mass for parallel sample filters (Figure S2).

A punch of 47 mm in diameter of filter sample was cut and fixed in a sand core funnel. A rubber tube was attached to the funnel outlet and blocked by water pressure. A volume of 50–200 mL (depended on the sample loadings of filters) distilled water was slowly injected into the funnel. The filter was immersed in water in

the funnel for 30 min. Then, the rubber tube at the funnel outlet was slowly released of pressure, and water in the funnel gently passed through the sample filter and drained out. Another volume of 50–200 mL water was added in the funnel and filtered out slowly. A small amount of ethanol was applied to remove remaining water in filter and funnel, and the AFD system was ready for next stage of organic solvent treatment.

The volume of 60 mL mixtures of dichloromethane (DCM) and acetone (1:1, *v*:*v*) was injected into the funnel, and held for 30 min before being filtered out. Small amounts of ethanol, then water, were employed to clean the funnel. The release of water pressure from the funnel outlet rubber tube should consistently be slow and ensure a gentle filtration. After that, the treated filter in the funnel was dried at 60°C. The solvent treatment and original sample filters were then stored in a desiccator before further analysis. Through the dissolution of organic and inorganic coatings, the solvent decoated, and therefore pure BC remained on the sample filter.

2.3. Determination of BC Mass and Optical Properties

The elemental carbon (EC, as the mass-based proxy for optical BC) and organic carbon (OC) loadings on the quartz filter samples were determined with the thermal-optical methods, and the EC is operationally defined as the carbon that volatilizes from filter samples at elevated temperatures in the presence of oxygen. A thermal-optical transmittance (TOT) and reflectance (TOR) carbon analyzer (Sunset Laboratory, Tigard, OR, USA) was employed. The temperature steps of NIOSH870 protocol and the TOT method were applied for this research [*Chen et al*., 2017; *Panteliadis et al*., 2015], which was slightly modified from our earlier study [*Chen et al*., 2013] and others [*Schauer et al*., 2003; *Subramanian et al*., 2006].

The light absorption of BC (EC) on filter samples was measured by the laser beam at wavelength 678 nm on the carbon analyzer. When the EC volatilized from the quartz filter sample, the intensity of transmitted light filter was simultaneously monitored. The light attenuation (ATN) was calculated from the transmission signal before (I) and after (I_0) EC burning out.

$$\mathrm{ATN} = -100 \cdot \ln\left(\frac{I}{I_0}\right) \tag{1}$$

The mass absorption cross section (MAC, unit in $m^2\ g^{-1}$) was calculated from the relationship between ATN and EC loading ($\mu g\ cm^{-2}$) on the filters [*Ram and Sarin*, 2009; *Weingartner et al*., 2003].

$$\mathrm{MAC} = \frac{\mathrm{ATN}}{\mathrm{EC} \cdot C \cdot R(\mathrm{ATN})} \tag{2}$$

Where C and R(ATN) are two empirical factors to correct the optical properties of filtered aerosols with the respect to the "real" aerosols in air.

R(ATN) corrects shadowing effect for aerosols collected on the filter. Weingartner and coauthors show that R(ATN) can be determined using a f variable [*Weingartner et al*., 2003].

$$R(\mathrm{ATN}) = \left(\frac{1}{f} - 1\right)\left(\frac{\ln \mathrm{ATN} - \ln 10}{\ln 50 - \ln 10}\right) + 1 \tag{3}$$

where f was calculated with the relationship

$$f = \alpha(1 - \omega_0) + 1 \tag{4}$$

where α stayed relatively constant for varied wavelengths with a value of 0.85 ± 0.05 at 660 nm (similar to the wavelength 678 nm of this study) [*Weingartner et al*., 2003]. The ω_o is the aerosol single-scattering albedo, which was monitored during the field campaign (supporting information S1). The original filter samples before AFD solvent treatment use the monitored ω_o for the calculation of f values. The linear correlation between EC and ATN in original samples increases from R^2 = 0.91 to R^2 = 0.96 after the correction

of R(ATN). The propagating error of R(ATN) for original samples was 21%, considering both uncertainties of α and ω_o.

Relatively pure BC remains on the filters after the solvent-aided dissolution of coating matters, and we apply a f value of fresh pure soot for the R(ATN) correction. The filtered fresh pure diesel soot and biomass soot show f values of 1.64 and 1.89 at 660 nm, respectively [*Weingartner et al*., 2003]. The f value decreases to 1.14–1.2 for mixtures of soot with organic carbon or sulfates. We thus applied a f value of 1.64 to correcting R(ATN) for solvent-decoated pure BC samples, considering the dominant sources of fossil fuel combustion for BC emissions in China [*Chen et al*., 2013]. The difference of f between 1.64 and 1.89 causes an uncertainty of 15%. The linear correlation between EC and ATN increases from R^2 = 0.91 to R^2 = 0.94 using such correction of R(ATN) for solvent treatment samples. In theory, the values of C primarily depend on the filter type [*Collaud Coen et al*., 2010; *Weingartner et al*., 2003]. All samples in this research use the same filter product, Pallflex, Tissuquartz 2500 QAT-UP. The C correction of 5.74 ± 0.94 was determined by standard diesel vehicle aerosols [*Chen et al*., 2017]. With this correction, the ECOC analyzer measurement of absorption coefficients generally agreed with an online Aethalometer monitoring (R^2 = 0.89 for the rural North China campaign).

Analysis of blank samples showed the detection limit of ATN of 0.8 (n = 19). The replicate analysis of original samples (n = 19) showed that uncertainties of EC and ATN were ~13% and ~10% (except one sample of 21%), respectively. Chow et al. report an uncertainty of 10% for ATN with a thermal-optical ECOC analyzer [*Chow et al*., 2004]. The propagated error of MAC (equation (2)) was 31% for original samples before treatment, considering uncertainties from EC, ATN, C, R(ATN), A, and V. Considering the proper correction of C and R(ATN) and good correlation between EC and ATN ($R^2 > 0.94$), the MAC error estimates should be the upper limits.

2.4. Enhancement of Mass Absorption Cross Section

The BC absorption enhancement (E_{MAC}) in ambient aerosols was measured as the ratio between BC MAC of original ambient samples ($MAC_{original}$) and that after their AFD solvent-decoating treatment ($MAC_{treated}$).

$$E_{MAC} = \frac{MAC_{original}}{MAC_{treated}} \tag{5}$$

The $PM_{2.5}$ samples at the rural North China site showed E_{MAC} in ranges of 2.25 ± 0.55. The E_{MAC} increases simultaneously (R^2 = 0.64) with the ratios of SO_4^{2-}/EC, and the E_{MAC} partly increases as a function of OC/EC ratios (R^2 = 0.3, Figure S3). The OC/EC ratio variations are controlled not only by the formation of secondary organic aerosols but also by the changes in emission sources. For example, the OC/EC ratio of barley straw burning aerosols (7.3) and rice straw burning emission (8.3) [*Ryu et al*., 2004] can be 10 times that (<1) of vehicle emissions [*Handler et al*., 2008]. The changes in emission sources contribute to the large variations of OC/EC ratios, and thus the ratio increase may not suggest forming secondary aerosol coating for absorption enhancement. On the other hand, sulfate aerosols are produced predominantly from atmospheric photochemical aging (secondary sources), and the coating effect on the BC absorption is indexed to SO_4^{2-}/EC ratios (Figure 1a). Sulfate concentrations during daytime were high in contrast to the low level of EC (Figure 1b), and the SO_4^{2-}/EC ratios were increased by photochemical production of secondary sulfate coating, which contributes to stronger absorption enhancement of BC aerosols for the daytime samples than nighttime samples (Figure 1c).

3. GISS Climate Modeling

The Goddard Institute for Space Studies (GISS) atmospheric general circulation model (GCM, Model E2 version) was employed to simulate BC radiative forcing [*Hansen et al*., 2002; *Schmidt et al*., 2006, 2014]. The simulation used the configuration similar to the Coupled Model Intercomparison Project Phase 5 (CMIP5) [*Schmidt et al*., 2014]. Resolution is 2° × 2.5° latitude by longitude in horizontal and vertically spans 40 layers with top at 0.1 hPa. The simulation included interactive chemistry, aerosols, and dust driven by emissions [*Koch et al*., 2011]. The descriptions of the tracer code, chemical reactions, species, and model evaluation are detailed in the literature [*Shindell et al*., 2006, 2013a].

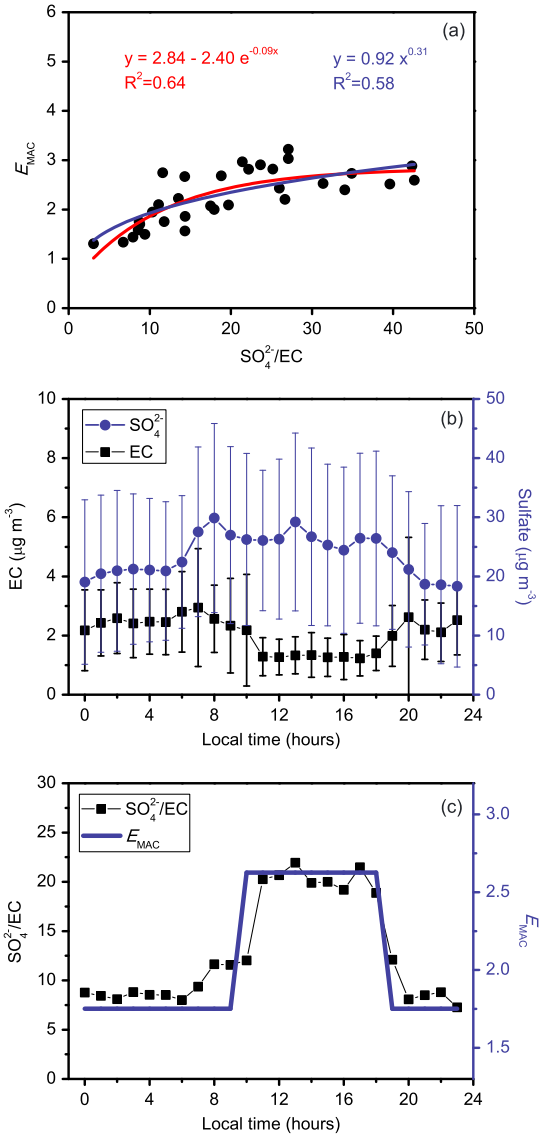

Figure 1. The relationship between E_{MAC} and SO_4^{2-}/EC ratios at the rural North China site. (a) The E_{MAC} regressions with SO_4^{2-}/EC ratios using exponential function and power law. (b) Diurnal pattern of EC and sulfate concentrations (the average and standard deviation of 21 day data from 1 h time resolution monitoring). (c) Daytime peaks of SO_4^{2-}/EC ratios (at 1 h time resolution), and the average of E_{MAC} for 21 day time samples and 21 nighttime samples.

The emission and climate forcing modeling of aerosol species primarily followed description in *Koch et al.* [2006], with updating to CMIP5 emissions of BC, OC, and SO_2 [*Lamarque et al.*, 2010; *Schmidt et al.*, 2014]. Aerosols are treated as externally mixed and have prescribed size and properties in the standard run of GISS model.

We then for a second run applied the observational absorption enhancement (E_{MAC}) to calculate BC radiative forcing in the climate model. The absorption enhancement of BC from fuel combustion sources is parameterized by the observed E_{MAC} regressions with SO_4^{2-}/EC ratios at the rural North China site (Figure 1a). In model calculation of E_{MAC}, we apply the regressions of exponential function (equation (6)) and power law (equation (7)) both display better correlation coefficient than linear regression (Figure S4).

$$y = 2.84–2.40\, e^{-0.09x} \quad (6)$$

$$y = 0.92\, x^{0.31} \quad (7)$$

where the independent variable x is SO_4^{2-}/EC ratios and the dependent variable y is E_{MAC}.

Figure 2a shows the map of aged BC of fuel combustion sources in predictions. The GISS_E2 simulations of BC concentrations have been evaluated from the Atmospheric Chemistry and Climate Model Intercomparison Project (ACCMIP), and the simulations tend to match observed concentrations in Europe, North America, Antarctic, Greenland, and at some sites on the Tibetan Plateau [*Lee et al.*, 2013]. The modeled sulfate loading, scaled to a global average of 3.65 mg m^{-2} to agree with CMIP5 simulation [*Lamarque et al.*, 2010] is shown in Figure 2c.

Open biomass burning BC (Figure 2b) contains only trace amounts of coemitted SO_2. Sulfate loading is low for open biomass burning sources, which occur mainly in tropical Africa and Amazon basin. The secondary organic aerosols are also insignificant in biomass burning source regions [*Aouizerats et al.*, 2015]. To configure open biomass burning BC, we use a constant E_{MAC} of 1.4 based on literature reports of BC absorption enhancement in biomass burning plumes [*Lack et al.*, 2012]. However, the enhancement factor was likely underestimated for the aged biomass burning plume or high relative humidity (RH) region.

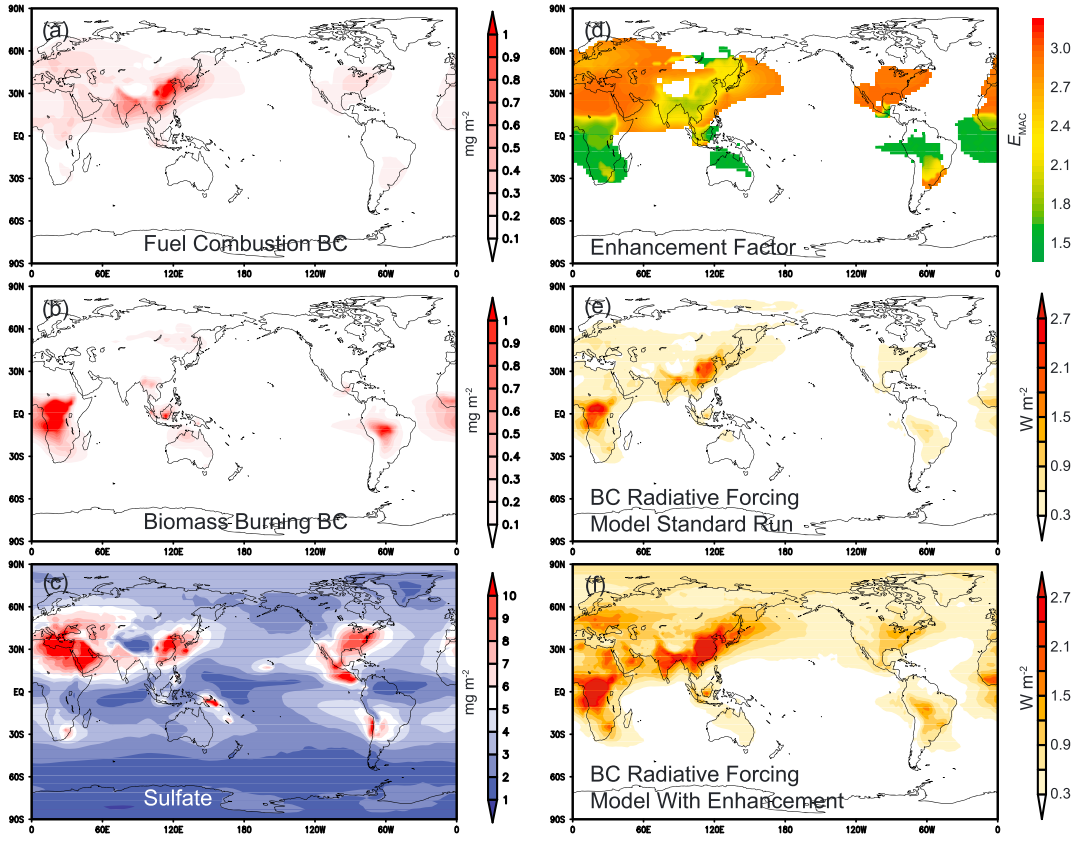

Figure 2. Model simulations of aerosols and BC absorption enhancement. (a) Aged BC mass loading from combustion of fossil fuel and biofuel; (b) open biomass burning BC; (c) sulfate aerosols; (d) observationally constrained enhancement of mass absorption cross section (E_{MAC}) of BC in GISS modeling, and only areas with BC mass loading larger than 0.1 mg m^{-2} are shown; (e) BC radiative forcing for standard run in CMIP5 GISS configuration; and (f) model configured with observational constraints of BC absorption enhancement.

Taken together, the modeled E_{MAC} and enhancement of BC radiative forcing with configuration of BC absorption enhancement using our observational constraints are named as "Model With Enhancement", while "Model Standard Run" represents standard configuration (no enhancement) in CMIP5 GISS model.

4. Climate Model Prediction

GCMs currently describe the E_{MAC} with three types of methods: no absorption enhancement (external mixing), fixed E_{MAC} (typically a factor of 1.5–2), or aerosol microphysics models using photochemical aging to simulate core-shell formation [*Bauer et al.*, 2013; *Chung and Seinfeld*, 2005; *Jacobson*, 2012; *Schulz et al.*, 2006]. Here the modeling result shows annual average E_{MAC} at a factor of 2 in East and South Asia (Figure 2d). The high levels of ambient BC in the atmosphere of East Asia (Figure 2a) have been apportioned to predominantly fossil fuel combustion [*Chen et al.*, 2013], whereas the sources to South Asian BC include a large contribution from biomass combustion [*Gustafsson et al.*, 2009; *Li et al.*, 2016]. The great SO_2 emissions from fuel combustion in industrially active regions [*Ohara et al.*, 2007] enable BC to mix with abundant secondary sulfate products (Figure 2c). Such sulfate-BC mixtures largely drove the absorption enhancement in populated and fossil-fueled areas such as North China. The climate model simulation, parameterized with the observed E_{MAC} constraints, identified a strong increase in BC radiative forcing (Figures 2e and 2f) for China where coemitted profiles and subsequent production of sulfate aerosols [*Wang et al.*, 2016] bring high enhancement effects.

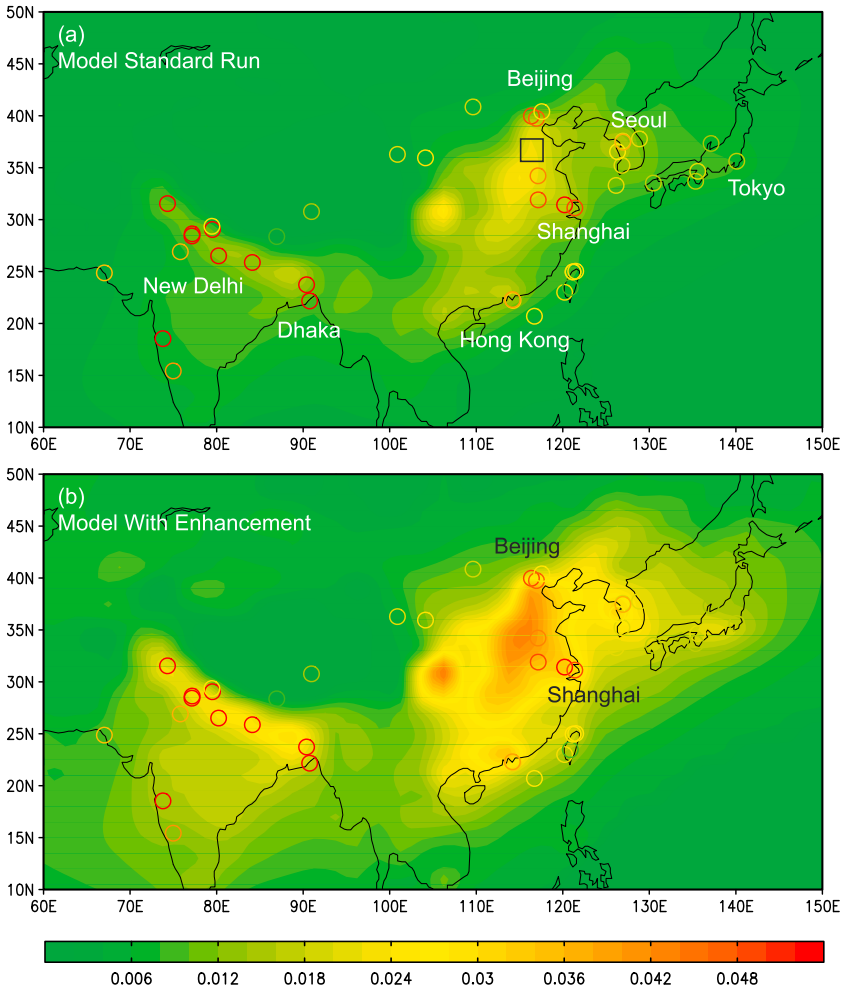

Figure 3. Annual absorption aerosol optical depth (AAOD) at 550 nm for BC loading from GISS model (a) in standard run and (b) with configuration of BC absorption enhancement using our observational constraints for the year 2000 conditions. The BC-AAOD retrieved for the AERONET sites are shown as circles following the same color scale as the model-based AAOD. The AERONET BC-AAOD is based on average inversion of data sampled during years 2000–2014 [*Dubovik et al.*, 2000]. The observation sites in North China are located in the area marked with a square in Figure 3a.

5. Improved Agreement Between Bottom-Up and Top-Down Estimates of BC Radiative Forcing

An important test is the comparison of the bottom-up prediction of aerosol absorption optical depth (AAOD) of the GISS model, with the improved configuration for E_{MAC}, with AERONET top-down observations of AAOD. Because the absorption enhancement factor is weakly impacted by wavelength [*Peng et al.*, 2016], the AAOD at 550 nm, which is different from the observed E_{MAC} at 678 nm, was compared due to the 550 nm wavelength simulated by many models. The model in standard configuration shows lower AAOD than AERONET observations by a factor of 2–3 (Figure 3a). In contrast, the here improved model configuration with observed E_{MAC} predicts larger AAOD, which improves the agreement with AERONET observations (Figure 3b). The agreement is particularly obvious in East Asia (Figure 4a), while we note that the configuration of BC absorption enhancement still causes some underestimation of AAOD in South Asia (Figure 4b).

In global scale (Figure 5), the model with configuration of observational E_{MAC} captured the AAOD of AERONET observations in North America and Europe. Similar to China, fossil fuel combustion in these industrialized areas emits high content of SO_2 [*Lamarque et al.*, 2010] that forms abundant secondary sulfate coatings on BC core, enhancing light absorption by a factor of ~2. On the other hand, Africa and South America (tropical

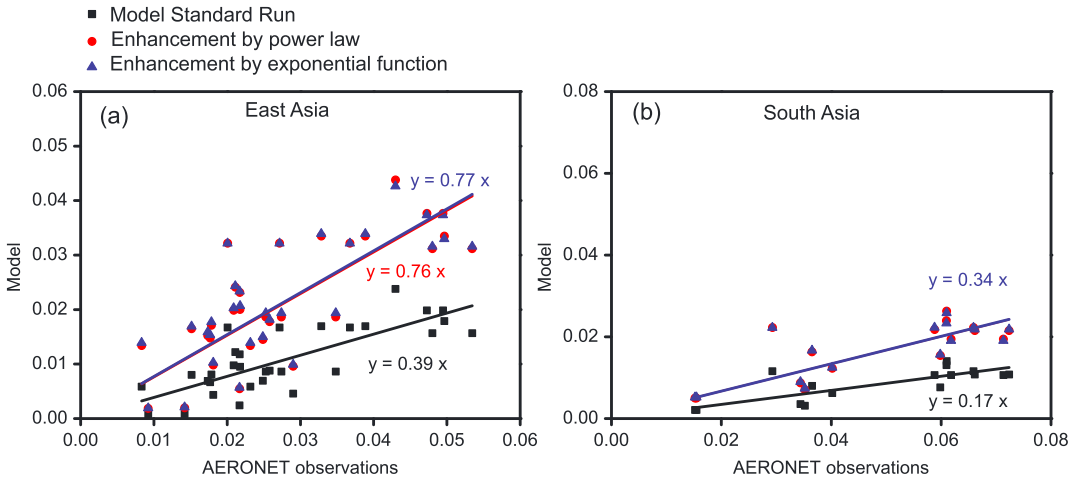

Figure 4. Absorption aerosol optical depth (AAOD) at 550 nm for BC loading retrieved from GISS model and AERONET observations in (a) East Asia and (b) South Asia. The model with enhancement was calculated by observed E_{MAC} regressions with SO_4^{2-}/EC ratios (Figure 1) follow a power law (red circles) and an exponential function (black triangles).

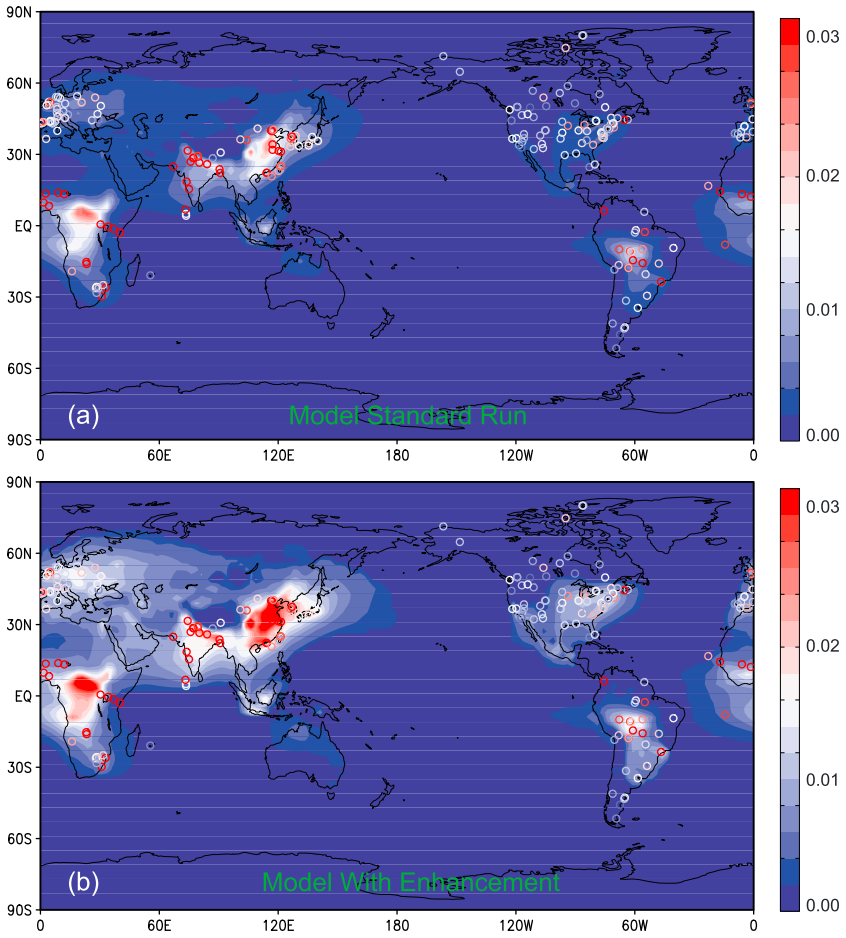

Figure 5. Global map of annual absorption aerosol optical depth (AAOD) at 550 nm for BC loading from GISS model (a) in standard run and (b) with configuration of BC absorption enhancement using our observational constraints for the year 2000 conditions. The BC-AAOD retrieved for the AERONET sites are shown as circles following the same color scale as the model-based AAOD.

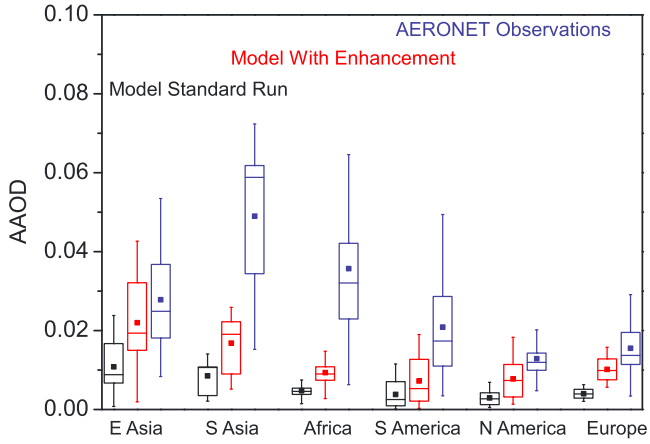

Figure 6. Comparisons of AAOD between model and AERONET observations in five regions. AAOD at 550 nm for BC loading from GISS model in standard run (black box and whisker plots) and with configuration of BC absorption enhancement using observational constraints (red box and whisker plots) are compared with that of AERONET observations (blue box and whisker plots). Box and whisker plots show the mean, median, lower and upper quartiles, and the 9th to 91st percentile ranges for data in each region.

forests) are dominated by biomass burning emissions, and the configuration of sulfate coating effect has little improvement for the model prediction for these areas. Biomass burning plume contains tar balls, which are important absorbers across the visible spectrum [*Jacobson*, 2012]. The tropic forests also have high RH, and water droplet may increase the BC absorption enhancement.

6. Discussion and Conclusion

The BC absorption enhancement from aerosol coatings in industrialized areas such as North China can be correctly predicted with the configuration of sulfate to BC mixing ratios. Sulfate aerosols have a major contribution to haze in North China, for example, sulfate concentrations were observed as high as ~300 μg m^{-3} during the January 2013 winter haze event in Beijing [*Cheng et al.*, 2016]. The severe pollution of sulfate and other secondary aerosols could significantly increase the BC absorption.

This observational constraint at a regional rural site could be representative for severely polluted area where the photochemical aging of anthropogenic gaseous pollutants such as SO_2, NO_x, NH_3, and VOCs form aerosol shells around the BC core. China is estimated to be the strongest source area for BC emissions with respect to energy-related combustion [*Bond et al.*, 2007; *Kurokawa et al.*, 2013]. The coemissions of BC, OC, and gaseous pollutants from industry and household coal consumption in densely populated areas in northern China cause air pollution at a regional scale [*Shang et al.*, 2017; *Zhang and Cao*, 2015].

The climate model using this parameterization constrained from the rural North China observations needs be improved for its global prediction. Ambient aerosol coating and BC absorption enhancement factors are expected to vary between energy-related combustion and open biomass burning. The absorption enhancement of ambient BC by a factor of 2 largely closes the earlier underestimation by the model relative to observations with respect to BC absorption of solar radiation in East Asia, North America, and Europe (Figure 6). Meanwhile, the model with absorption enhancement by a factor 2 still underpredicts AAOD in South Asia compared to the AERONET observations in the region. Biomass burning is an important source of air pollutants in South Asia, and including tar ball absorption should improve the model performance.

The absorption enhancement by a factor 1.4 in biomass burning source areas such as Africa and Amazon Basin was underestimated. The emission inventories for biomass burning BC have large uncertainties; for example, biomass burning BC in Africa from AMMABB inventory (2.3 TgC) is twice of GFEDv2 emission (0.95 TgC) [*Liousse et al.*, 2010]. GFEDv2 inventory is used as input data for the construction of biomass burning emission in CMIP5 simulation for year 2000 condition [*Lamarque et al.*, 2010]. High-resolution inventories for biomass burning emission are available at a regional scale rather than globally, e.g., *Cohen* [2014]. Moreover, light absorption by organic aerosol due to the presence of brown carbon or tar ball has yet to be resolved in current GISS model and other CMIP5 simulations. Biomass burning is the dominant source of brown carbon [*Saleh et al.*, 2015; *Washenfelder et al.*, 2015]; thus, brown carbon absorption due to emissions from savanna fires in Africa and forest fires in Amazon Basin may reduce the gap between existing model-based and observationally constrained estimates of radiative absorption. The model prediction for South Asia, Africa, and Amazon Basin should be constrained from the coating observation in biomass burning source areas.

Acknowledgments
This research has received funding from the National Natural Science Foundation of China (21647006 and 91644214) and State Key Laboratory of Cryospheric Science (SKLCS-OP-2017-01). We thank AERONET principal investigators and their staff for establishing and maintaining the networks used in this investigation. Brent Holben and David M Giles provided useful support and advice on AAOD. The data used are listed in the references, tables, and supporting information. AERONET AAOD is available at http://aeronet.gsfc.nasa.gov/. NASA-GISS GCM and associated model input data were downloaded from the repository at https://www.giss.nasa.gov/projects/gcm/.

References

Andreae, M. O., and V. Ramanathan (2013), Climate's dark forcings, *Science*, *340*(6130), 280–281, doi:10.1126/science.1235731.

Aouizerats, B., G. R. van der Werf, R. Balasubramanian, and R. Betha (2015), Importance of transboundary transport of biomass burning emissions to regional air quality in Southeast Asia during a high fire event, *Atmos. Chem. Phys.*, *15*(1), 363–373, doi:10.5194/acp-15-363-2015.

Bauer, S. E., A. Ault, and K. A. Prather (2013), Evaluation of aerosol mixing state classes in the GISS modelE-MATRIX climate model using single-particle mass spectrometry measurements, *J. Geophys. Res. Atmos.*, *118*, 9834–9844, doi:10.1002/jgrd.50700.

Bond, T. C., E. Bhardwaj, R. Dong, R. Jogani, S. Jung, C. Roden, D. G. Streets, and N. M. Trautmann (2007), Historical emissions of black and organic carbon aerosol from energy-related combustion, 1850–2000, *Global Biogeochem. Cycles*, *21*, GB2018, doi:10.1029/2006GB002840.

Cappa, C. D., et al. (2012), Radiative absorption enhancements due to the mixing state of atmospheric clack carbon, *Science*, *337*(6098), 1078–1081, doi:10.1126/science.1223447.

Chen, B., et al. (2013), Source forensics of black carbon aerosols from China, *Environ. Sci. Technol.*, *47*(16), 9102–9108, doi:10.1021/es401599r.

Chen, B., Z. Bai, X. Cui, J. Chen, A. Andersson, and Ö. Gustafsson (2017), Light absorption enhancement of black carbon from urban haze in northern China winter, *Environ. Pollut.*, *221*, 418–426, doi:10.1016/j.envpol.2016.12.004.

Cheng, Y., et al. (2016), Reactive nitrogen chemistry in aerosol water as a source of sulfate during haze events in China, *Sci. Adv.*, *2*(12), e1601530, doi:10.1126/sciadv.1601530.

Chow, J. C., J. G. Watson, L. W. A. Chen, W. P. Arnott, H. Moosmüller, and K. Fung (2004), Equivalence of elemental carbon by thermal/optical reflectance and transmittance with different temperature protocols, *Environ. Sci. Technol.*, *38*(16), 4414–4422, doi:10.1021/es034936u.

Chung, S. H., and J. H. Seinfeld (2005), Climate response of direct radiative forcing of anthropogenic black carbon, *J. Geophys. Res.*, *110*, D11102, doi:10.1029/2004JD005441.

Cohen, J. B. (2014), Quantifying the occurrence and magnitude of the Southeast Asian fire climatology, *Environ. Res. Lett.*, *9*(11) 114018.

Cohen, J. B., and R. G. Prinn (2011), Development of a fast, urban chemistry metamodel for inclusion in global models, *Atmos. Chem. Phys.*, *11*(15), 7629–7656.

Cohen, J. B., and C. Wang (2014), Estimating global black carbon emissions using a top-down Kalman filter approach, *J. Geophys. Res. Atmos.*, *119*, 307–323, doi:10.1002/2013JD019912.

Cohen, J. B., R. G. Prinn, and C. Wang (2011), The impact of detailed urban-scale processing on the composition, distribution, and radiative forcing of anthropogenic aerosols, *Geophys. Res. Lett.*, *38*, L10808, doi:10.1029/2011GL047417.

Collaud Coen, M., et al. (2010), Minimizing light absorption measurement artifacts of the Aethalometer: Evaluation of five correction algorithms, *Atmos. Meas. Tech.*, *3*(2), 457–474, doi:10.5194/amt-3-457-2010.

Du, H., L. Kong, T. Cheng, J. Chen, J. Du, L. Li, X. Xia, C. Leng, and G. Huang (2011), Insights into summertime haze pollution events over Shanghai based on online water-soluble ionic composition of aerosols, *Atmos. Environ.*, *45*(29), 5131–5137, doi:10.1016/j.atmosenv.2011.06.027.

Dubovik, O., A. Smirnov, B. N. Holben, M. D. King, Y. J. Kaufman, T. F. Eck, and I. Slutsker (2000), Accuracy assessments of aerosol optical properties retrieved from Aerosol Robotic Network (AERONET) Sun and sky radiance measurements, *J. Geophys. Res.*, *105*(D8), 9791–9806, doi:10.1029/2000JD900040.

Fierce, L., T. C. Bond, S. E. Bauer, F. Mena, and N. Riemer (2016), Black carbon absorption at the global scale is affected by particle-scale diversity in composition, *Nat. Commun.*, *7*, 12361, doi:10.1038/ncomms12361.

Gustafsson, Ö., and V. Ramanathan (2016), Convergence on climate warming by black carbon aerosols, *Proc. Natl. Acad. Sci. U.S.A.*, *113*(16), 4243–4245, doi:10.1073/pnas.1603570113.

Gustafsson, Ö., M. Kruså, Z. Zencak, R. J. Sheesley, L. Granat, E. Engström, P. S. Praveen, P. S. P. Rao, C. Leck, and H. Rodhe (2009), Brown clouds over South Asia: Biomass or fossil fuel combustion?, *Science*, *323*(5913), 495–498, doi:10.1126/science.1164857.

Handler, M., C. Puls, J. Zbiral, I. Marr, H. Puxbaum, and A. Limbeck (2008), Size and composition of particulate emissions from motor vehicles in the Kaisermühlen-tunnel, Vienna, *Atmos. Environ.*, *42*(9), 2173–2186, doi:10.1016/j.atmosenv.2007.11.054.

Hansen, J., et al. (2002), Climate forcings in Goddard Institute for Space Studies SI2000 simulations, *J. Geophys. Res.*, *107*(D18), 4347, doi:10.1029/2001JD001143.

He, C., et al. (2014), A global 3-D CTM evaluation of black carbon in the Tibetan Plateau, *Atmos. Chem. Phys.*, *14*(13), 7091–7112, doi:10.5194/acp-14-7091-2014.

Jacobson, M. Z. (2000), A physically-based treatment of elemental carbon optics: Implications for global direct forcing of aerosols, *Geophys. Res. Lett.*, *27*(2), 217–220, doi:10.1029/1999GL010968.

Jacobson, M. Z. (2001), Strong radiative heating due to the mixing state of black carbon in atmospheric aerosols, *Nature*, *409*(6821), 695–697, doi:10.1038/35055518.

Jacobson, M. Z. (2012), Investigating cloud absorption effects: Global absorption properties of black carbon, tar balls, and soil dust in clouds and aerosols, *J. Geophys. Res.*, *117*, D06205, doi:10.1029/2011JD017218.

Koch, D., G. A. Schmidt, and C. V. Field (2006), Sulfur, sea salt, and radionuclide aerosols in GISS ModelE, *J. Geophys. Res.*, *111*, D06206, doi:10.1029/2004JD005550.

Koch, D., et al. (2011), Coupled aerosol–chemistry–climate twentieth-century transient model investigation: Trends in short-lived species and climate rResponses, *J. Clim.*, *24*(11), 2693–2714, doi:10.1175/2011jcli3582.1.

Koch, D., et al. (2009), Evaluation of black carbon estimations in global aerosol models, *Atmos. Chem. Phys.*, *9*(22), 9001–9026, doi:10.5194/acp-9-9001-2009.

Kurokawa, J., T. Ohara, T. Morikawa, S. Hanayama, G. Janssens-Maenhout, T. Fukui, K. Kawashima, and H. Akimoto (2013), Emissions of air pollutants and greenhouse gases over Asian regions during 2000–2008: Regional Emission inventory in ASia (REAS) version 2, *Atmos. Chem. Phys.*, *13*(21), 11,019–11,058, doi:10.5194/acp-13-11019-2013.

Lack, D. A., J. M. Langridge, R. Bahreini, C. D. Cappa, A. M. Middlebrook, and J. P. Schwarz (2012), Brown carbon and internal mixing in biomass burning particles, *Proc. Natl. Acad. Sci. U.S.A.*, *109*(37), 14802–14807, doi:10.1073/pnas.1206575109.

Lamarque, J. F., et al. (2010), Historical (1850–2000) gridded anthropogenic and biomass burning emissions of reactive gases and aerosols: Methodology and application, *Atmos. Chem. Phys.*, *10*(15), 7017–7039, doi:10.5194/acp-10-7017-2010.

Lee, Y. H., et al. (2013), Evaluation of preindustrial to present-day black carbon and its albedo forcing from Atmospheric Chemistry and Climate Model Intercomparison Project (ACCMIP), *Atmos. Chem. Phys.*, *13*(5), 2607–2634, doi:10.5194/acp-13-2607-2013.

Li, C., C. Bosch, S. Kang, A. Andersson, P. Chen, Q. Zhang, Z. Cong, B. Chen, D. Qin, and Ö. Gustafsson (2016), Sources of black carbon to the Himalayan–Tibetan Plateau glaciers, *Nat. Commun.*, *7*, 12574, doi:10.1038/ncomms12574.

Liousse, C., et al. (2010), Updated African biomass burning emission inventories in the framework of the AMMA-IDAF program, with an evaluation of combustion aerosols, *Atmos. Chem. Phys.*, *10*(19), 9631–9646, doi:10.5194/acp-10-9631-2010.

Lu, Z., Q. Zhang, and D. G. Streets (2011), Sulfur dioxide and primary carbonaceous aerosol emissions in China and India, 1996–2010, *Atmos. Chem. Phys.*, *11*(18), 9839–9864, doi:10.5194/acp-11-9839-2011.

Matsui, H. (2016), Black carbon simulations using a size- and mixing-state-resolved three-dimensional model: 1. Radiative effects and their uncertainties, *J. Geophys. Res. Atmos.*, *121*, 1793–1807, doi:10.1002/2015JD023998.

Ohara, T., H. Akimoto, J. Kurokawa, N. Horii, K. Yamaji, X. Yan, and T. Hayasaka (2007), An Asian emission inventory of anthropogenic emission sources for the period 1980–2020, *Atmos. Chem. Phys.*, *7*(16), 4419–4444, doi:10.5194/acp-7-4419-2007.

Panteliadis, P., et al. (2015), ECOC comparison exercise with identical thermal protocols after temperature offset correction—Instrument diagnostics by in-depth evaluation of operational parameters, *Atmos. Meas. Tech.*, *8*(2), 779–792, doi:10.5194/amt-8-779-2015.

Peng, J., et al. (2016), Markedly enhanced absorption and direct radiative forcing of black carbon under polluted urban environments, *Proc. Natl. Acad. Sci. U.S.A.*, *113*(16), 4266–4271, doi:10.1073/pnas.1602310113.

Qin, Y., and S. D. Xie (2012), Spatial and temporal variation of anthropogenic black carbon emissions in China for the period 1980–2009, *Atmos. Chem. Phys.*, *12*(11), 4825–4841, doi:10.5194/acp-12-4825-2012.

Rajput, P., and M. M. Sarin (2014), Polar and non-polar organic aerosols from large-scale agricultural-waste burning emissions in northern India: Implications to organic mass-to-organic carbon ratio, *Chemosphere*, *103*, 74–79, doi:10.1016/j.chemosphere.2013.11.028.

Ram, K., and M. M. Sarin (2009), Absorption coefficient and site-specific mass absorption efficiency of elemental carbon in aerosols over urban, rural, and high-altitude sites in India, *Environ. Sci. Technol.*, *43*(21), 8233–8239, doi:10.1021/es9011542.

Ryu, S. Y., J. E. Kim, H. Zhuanshi, Y. J. Kim, and G. U. Kang (2004), Chemical composition of post-harvest biomass burning aerosols in Gwangju, Korea, *J. Air Waste Manag. Assoc.*, *54*(9), 1124–1137, doi:10.1080/10473289.2004.10471018.

Saleh, R., M. Marks, J. Heo, P. J. Adams, N. M. Donahue, and A. L. Robinson (2015), Contribution of brown carbon and lensing to the direct radiative effect of carbonaceous aerosols from biomass and biofuel burning emissions, *J. Geophys. Res. Atmos.*, *120*, 10,285–10,296, doi:10.1002/2015JD023697.

Schauer, J. J., et al. (2003), ACE-Asia intercomparison of a thermal-optical method for the determination of particle-phase organic and elemental carbon, *Environ. Sci. Technol.*, *37*(5), 993–1001, doi:10.1021/es020622f.

Schmidt, G. A., et al. (2006), Present-day atmospheric simulations using GISS ModelE: Comparison to in situ, satellite, and reanalysis data, *J. Clim.*, *19*(2), 153–192, doi:10.1175/jcli3612.1.

Schmidt, G. A., et al. (2014), Configuration and assessment of the GISS ModelE2 contributions to the CMIP5 archive, *J. Adv. Model. Earth Syst.*, *6*(1), 141–184, doi:10.1002/2013ms000265.

Schulz, M., et al. (2006), Radiative forcing by aerosols as derived from the AeroCom present-day and pre-industrial simulations, *Atmos. Chem. Phys.*, *6*(12), 5225–5246, doi:10.5194/acp-6-5225-2006.

Shang, H., L. Chen, H. Letu, M. Zhao, S. Li, and S. Bao (2017), Development of a daytime cloud and haze detection algorithm for Himawari-8 satellite measurements over central and eastern China, *J. Geophys. Res. Atmos.*, *122*, 3528–3543, doi:10.1002/2016JD025659.

Shindell, D., et al. (2006), Simulations of preindustrial, present-day, and 2100 conditions in the NASA GISS composition and climate model G-PUCCINI, *Atmos. Chem. Phys.*, *6*(12), 4427–4459, doi:10.5194/acp-6-4427-2006.

Shindell, D. T., et al. (2013a), Interactive ozone and methane chemistry in GISS-E2 historical and future climate simulations, *Atmos. Chem. Phys.*, *13*(5), 2653–2689, doi:10.5194/acp-13-2653-2013.

Shindell, D. T., et al. (2013b), Radiative forcing in the ACCMIP historical and future climate simulations, *Atmos. Chem. Phys.*, *13*(6), 2939–2974, doi:10.5194/acp-13-2939-2013.

Subramanian, R., A. Y. Khlystov, and A. L. Robinson (2006), Effect of peak inert-mode temperature on elemental carbon measured using thermal-optical analysis, *Aerosol Sci. Technol.*, *40*(10), 763–780, doi:10.1080/02786820600714403.

Wang, G., et al. (2016), Persistent sulfate formation from London fog to Chinese haze, *Proc. Natl. Acad. Sci. U.S.A.*, *113*(48), 13,630–13,635, doi:10.1073/pnas.1616540113.

Washenfelder, R. A., et al. (2015), Biomass burning dominates brown carbon absorption in the rural southeastern United States, *Geophys. Res. Lett.*, *42*, 653–664, doi:10.1002/2014GL062444.

Weingartner, E., H. Saathoff, M. Schnaiter, N. Streit, B. Bitnar, and U. Baltensperger (2003), Absorption of light by soot particles: Determination of the absorption coefficient by means of aethalometers, *J. Aerosol Sci.*, *34*(10), 1445–1463, doi:10.1016/S0021-8502(03)00359-8.

Zhang, L., et al. (2015), Constraining black carbon aerosol over Asia using OMI aerosol absorption optical depth and the adjoint of GEOS-Chem, *Atmos. Chem. Phys.*, *15*(18), 10281–10308, doi:10.5194/acp-15-10281-2015.

Zhang, Y.-L., and F. Cao (2015), Fine particulate matter (PM2.5) in China at a city level, *Sci. Rep.*, *5*, 14884, doi:10.1038/srep14884.